Cement and Concrete Research 127 (2020) 105930

Contents lists available at ScienceDirect

Cement and Concrete Research

journal homepage: www.elsevier.com/locate/cemconres

Concrete mixing truck as a rheometer

Jon Elvar Wallevik[a,*], Olafur Haralds Wallevik[a,b]

[a] ICI Rheocenter, Innovation Center Iceland, Arleynir 2, Reykjavik IS-112, Iceland
[b] Reykjavik University, Menntavegi 1, Reykjavik IS-102, Iceland

ARTICLE INFO

Keywords:
Truck mixer
Rheology
Bingham model
Fresh concrete
CFD

ABSTRACT

An increasing interest has emerged in correlating the output of the concrete mixing truck to values obtained by rotational rheometers. The output of the former has usually been the hydraulic pressure needed to turn the drum. In such research, experimental errors can be higher than usual, which makes it harder to obtain confident relationships. To better understand the physical characteristics of the truck's rheological values, the above analysis is made by a series of computer simulations (i.e. with CFD). From this, it is evident that the slope H of the truck's pressure values depends both on the plastic viscosity μ as well as on the yield stress τ_0. However, for the intercept G of the truck's values, it is mostly dependent on the yield stress τ_0. In addition to this, both values H and G depend on volume of concrete in the truck as well as on density.

1. Introduction

The quality of concrete structures depends on the quality of each constituent used in the concrete mix. However, this is not the only controlling factor. The quality also depends on the rheological properties of the fresh concrete during casting into the formwork [1]. That is, concrete must be able to properly flow into all corners of the mold or formwork to fill it completely, with or without external consolidation depending on workability class. Tragic events may sometimes be traced back to concrete of unsuitable consistency resulting in, for example, coldjoint and honeycombing. Therefore, one of the primary criteria for a good concrete structure is that the fresh concrete has satisfactory rheological properties during casting [1]. The use of simulation of flow to analyze such behavior is something that has been increasing in popularity for the last decade [2-9]. In 2014, a RILEM state-of-the art report (TC 222–SCF) was made specifically on this subject [10]. Here, such a method is used to analyze the power required to turn (i.e. spin) the drum of a concrete mixing truck (also named *concrete truck mixer*, or *concrete mixer truck*, among other designations) for a wide range of different cases. It should be clear that utilizing simulation techniques is not limited to the above cases. Analysis of thixotropic behavior, formwork pressure, computer aided engineering and concrete mixing process are all examples of different computational applications used in concrete science [11-15].

In general, rotational rheometers have never been particularly popular at a jobsite. They are however well suited for laboratory use as they measure concrete consistency either in terms of fundamental physical quantities, namely yield stress τ_0 and plastic viscosity μ (assuming Bingham behavior) or some uncalibrated derivative thereof, usually designated as G and H values. In contrast to rheometers, the slump cone test (ASTM C143) is by far the most accepted tool for measuring consistency at a jobsite, which can be attributed to its simplicity in handling [16].

For the last few decades or so, an increasing interest has emerged in correlating the output of the concrete mixing truck to values obtained by rotational rheometers [17-20]. Such an output is either in the load imposed on the drive motor in watts or the hydraulic pressure needed to turn the drum, but this is something that depends on manufacturer [17]. Since the hydraulic pressure is related to movement of piston(s) inside the drum drive motor, work is being conducted (over a time interval), meaning that the pressure is related to power (i.e. rate of work). Historically, it is the hydraulic pressure that has been used to obtain values from the concrete mixing truck. But in either case of watt meter or hydraulic pressure the concept is the same and known as the "slump meter" [17].

In the attempt to correlate values from the "slump meter" to values from the rotational rheometer, experimental errors can be higher than usual, which makes it harder to obtain confident relationships between the two devices. These errors may originate from incorrect truck sampling, insufficient mixing time after addition of chemical admixtures and so forth [20]. In addition to this, possible errors from the rotational rheometer could be superimposed, which would make the overall research even more difficult.

The current work is undertaken to better understand the physical

* Corresponding author.
E-mail address: jon.w@innovation.is (J.E. Wallevik).

https://doi.org/10.1016/j.cemconres.2019.105930
Received 19 July 2019; Received in revised form 25 October 2019; Accepted 26 October 2019
Available online 05 November 2019

characteristics of the truck's rheological values and thus the feasibility in using the vehicle as a rheometer. The analysis is done by applying series of computer simulations (i.e. computational fluid dynamics - CFD). With this, the overall test environment is absolutely controlled and the above mentioned experimental error is avoided, thus allowing the truck's true potential to be examined. However, numerical errors can occur if computational techniques are incorrectly applied [21]. With that said, the current data is obtained from the simulation results presented in Ref. [14]. There, a good numerical quality was established to whatever extent possible.

2. Experimental and numerical setup

2.1. Overall test setup

In this work, the power required (in kilowatts) to rotate the drum in a concrete mixing truck is calculated as a function of different values of yield stress τ_0, plastic viscosity μ and drum charge volume V. In addition to this, power is calculated as a function of drum rotational speed f. More specifically, the drum rotational speed is set at $f = 0.03$, 0.07, 0.11, 015, 019 and 0.23 rps (revolutions per seconds), the drum charge volume is either at $V = 2.5\ m^3$, $5.4\ m^3$ or $8.2\ m^3$, the yield stress is set at $\tau_0 = 0$, 150 and 300 Pa, and the plastic viscosity is at $\mu = 25$, 75 and 125 Pa·s. Most of the cases with zero yield stress signify self-compacting concrete (see Figs. 11 and 12 in Ref. [22]), while cases with a larger yield stress represents concretes of the more conventional type [22].

Resulting in more than 160 simulations, the computational requirement to obtain the complete data was more than 150,000 CPU hours [14]. The resources were provided by the Icelandic High Performance Computing (IHPC) and the simulation software used was OpenFOAM [23].

As mentioned earlier, the same simulation results (i.e. calculated velocity **U**, shear rate $\dot{\gamma}$, volume fraction of concrete α_1 etc.) are used in this work as in Ref. [14]. As such, the explanation of the numerical techniques used, mesh quality, boundary conditions, accuracy of results etc., are here kept to minimum and the interested reader is rather referred to Ref. [14].

2.2. Geometry of the drum

The concrete drum under consideration is commercially available and produced in Germany. Its geometry is shown in Ref. [14], but an additional illustration is also shown here with Fig. 1. Naturally, the results presented in this work are relative to this specific drum geometry.

The total drum volume is $15.7\ m^3$, but the max rated drum capacity is $9\ m^3$. The max drum diameter is 2.3 m, while its length is about 5.2 m. The internal geometry consists of two helically shaped blades, in which the blade thickness is roughly 8 mm, while the height is about 430 mm (see also Ref. [14]). The space between two neighboring blades is 620 mm on average. The nominal range of drum speed is between 0 and 14 rpm (i.e. from 0 to 0.23 rps). For further information about the drum geometry and its mesh, see Ref. [14].

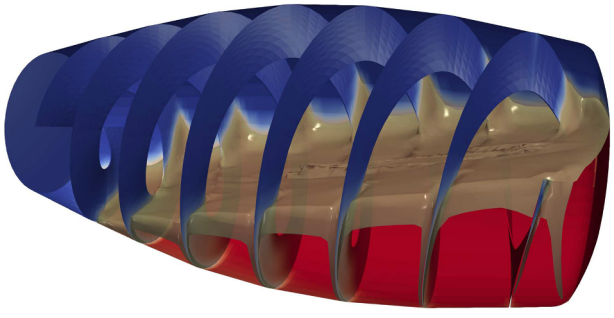

Fig. 1. The concrete drum under consideration, filled with about $5.4\ m^3$ of fresh concrete.

2.3. Atmospheric air and fresh concrete

For the current analysis, it is important to divide the drum's internal volume between the atmospheric air and the fresh concrete, which is done within the framework of Volume of Fluid (VOF) [24]. The volume fraction of fresh concrete within each computational cell is represented with α_1, while the volume fraction of atmospheric air is represented with α_2. Relative to Fig. 1, the upper part of the drum consists of cells with $\alpha_1 = 0$ and $\alpha_2 = 1$ (meaning air), while the lower part of the drum consists of cells with $\alpha_1 = 1$ and $\alpha_2 = 0$ (meaning concrete). For the interface between air and concrete, the following applies $0 < \alpha_1 < 1$. The volume fractions α_1 and α_2 are conserved in the sense that in each and every computational cell, the following is always valid $\alpha_1 + \alpha_2 = 1$.

The density ρ and apparent viscosity η are weighted by the volume fractions α_1 and α_2, given by Eqs. (1) and (2) [24-26]

$$\rho = \rho_1\ \alpha_1 + \rho_2\ \alpha_2, \tag{1}$$

$$\eta = \eta_1\ \alpha_1 + \eta_2\ \alpha_2. \tag{2}$$

In Eq. (1), the density of the concrete samples is set as $\rho_1 = 2350\ kg/m^3$, while for the atmospheric air it is set as $\rho_2 = 1.22\ kg/m^3$.

2.4. Constitutive equation

When using the Bingham viscoplastic fluid (or similar, like the Herschel-Bulkley fluid or the modified Bingham fluid [27]), the constitutive equation must consist of the Generalized Newtonian Model [28], or in short GNM, which is given by [28,29]:

$$\mathbf{T} = 2\ \eta\ \dot{\boldsymbol{\varepsilon}}. \tag{3}$$

The term $\dot{\boldsymbol{\varepsilon}} = \frac{1}{2}(\nabla\mathbf{U} + (\nabla\mathbf{U})^{\mathrm{T}})$ is known as the rate-of-deformation tensor [28-31]. Here, the apparent viscosity η is given by Eq. (2), in which the fresh concrete (the lower half part in Fig. 1) is modeled as a Bingham viscoplastic fluid,

$$\eta_1 = \mu + \frac{\tau_0}{\dot{\gamma}}, \tag{4}$$

while the atmospheric air (the upper half part in Fig. 1) is set as a Newtonian fluid with a constant viscosity equal to $\eta_2 = 1.78 \cdot 10^{-5}$ Pa·s. The computational implementation of η_1 into the source code is achieved by the regularization approach [21,27,32-36].

3. Data analysis

3.1. Calculation of mechanical power

The power (also, *mechanical power*, or *rate of work*) for a material body of volume V (also, *material volume*) is given by the following equation [31,35,37-39]:

$$\dot{W} = \int_V \rho\ \mathbf{g}\cdot\mathbf{U}\ dV + \int_A \mathbf{t}\cdot\mathbf{U}\ dA. \tag{5}$$

The term A represents the bounding surface (i.e. the boundary) of the volume V. The material body V in the above integrand is here chosen as the volume of the concrete sample inside the drum, namely either as $V = 2.5\ m^3$, $5.4\ m^3$ or $8.2\ m^3$. As such, the term $\dot{W}$ represents the rate of work (i.e. power) exerted by the drum in moving/shuffling/rotating/deforming the concrete inside it.

As already indicated, the terms ρ, **g** and **U** are the density [kg/m^3], gravity [m/s^2] and velocity [m/s], respectively. The term $\mathbf{t} = \mathbf{n}\cdot\boldsymbol{\sigma}$ is named traction and describes the force per unit area [N/m^2] applied at the boundary A, from the outer surroundings of the material volume V (i.e. in this case, applied by the steel drum wall, onto the fresh concrete). The term $\boldsymbol{\sigma} = -p\ \mathbf{I} + \mathbf{T}$ is the (total) stress tensor, in which **T** is

the extra stress tensor [Pa] (see Section 2.4), p is the pressure [Pa] and $\mathbf{I}$ is the unit dyadic. The term $\mathbf{n}$ is a unit normal vector located at the boundary A, pointing away from the material volume V [28-31,37,38].

As shown in Ref. [35] (pp. 386–389), through the mechanical energy equation, Eq. (5) can be transformed into Eq. (6). It should be noted that the time derivative in the latter is the total derivative (also, *material derivative*).

$$\dot{W}(t) = \int_V \rho \frac{d}{dt}\left[\frac{\mathbf{U}\cdot\mathbf{U}}{2}\right] dV + \int_V \eta\, \dot{\gamma}^2\, dV = \dot{W}_{KE}(t) + \dot{W}_{\eta}(t) \tag{6}$$

The variables $\dot{W}_{KE}(t)$ and $\dot{W}_{\eta}(t)$ represent the rate of work from the kinetic contribution and from the viscous contribution, respectively. For three dimensional incompressible flow where the GNM is valid (see Section 2.4), it can be shown that the shear rate in Eq. (6) is correctly calculated as [40]. This variable is highly non-uniform within the drum, meaning $\dot{\gamma} = \dot{\gamma}(x, y, z, t)$ (see Ref. [14], Fig. 3). The same applies for the velocity $\mathbf{U} = \mathbf{U}(x,y,z,t)$ as well as for the apparent viscosity $\eta = \eta(x,y,z,t)$, given by Eq. (2).

As mentioned in Ref. [14] (Section 2.6), to account for the drum rotation, the computer simulations are done by using the so-called single reference frame (SRF) approach [41]. This means that the obtained velocity $\mathbf{U} = \mathbf{U}_r$ is relative to a rotating frame of reference (see Eq. (6) in Ref. [14]). Since Eqs. (5) and (6) apply in the (stationary) inertial reference frame, the velocity must correspond to that frame of reference, meaning $\mathbf{U} = \mathbf{U}_r + \boldsymbol{\omega} \times \mathbf{x}$ in these two equations (the term $\boldsymbol{\omega}$ is the drum angular velocity and $\mathbf{x}$ is location [14,42]). However, it should be noted that since the shear rate $\dot{\gamma}$ is an invariant (see Section 4.7.2.1 in Ref. [21]), the value of $\dot{W}_{\eta}(t)$ in Eq. (6) is unaffected irrespective of calculation in the SRF or in the inertial reference frame.

3.2. Nominal drum charge volume

As already mentioned, the term V designates the volume of the concrete sample inside the drum. The drum charge volume V is nominally equal to either 2.5 m^3, 5.4 m^3 or 8.2 m^3. However, the actual value of V used in the volume integral Eq. (6), will differ slightly from nominal values, depending on how much concrete gets stuck on the drum steel boundary. More precisely, the concrete that gets stuck on the upper half part in Fig. 1 (i.e. on the steel boundary on the side of the atmospheric air) is not included in the volume integral Eq. (6). The same approach was used for the volume integration in Ref. [14] (see Section 3).

The amount of concrete that becomes stuck in the manner explained above, depends here primarily on the plastic viscosity μ. For the cases of the lowest plastic viscosity (25 Pa ·s), the volume used in the integration Eq. (6) is roughly 2% higher than the above mentioned nominal values. However, in the cases of highest plastic viscosity (125 Pa·s), the volume used is about 2% lower than the nominal values (meaning that more concrete is stuck on the upper half part in Fig. 1). In the intermediate case (75 Pa·s), the volume used in Eq. (6) is closest to the nominal values, namely 2.5 m^3, 5.4 m^3 or 8.2 m^3.

3.3. Case examples

Fig. 2 shows an example of the rate of work by Eq. (6), plotted as a function of time for the case of drum charge volume of $V = 2.5$ m^3 and different drum rotational speeds f. This figure applies for the more computationally challenging case, namely when the yield stress is $\tau_0 = 300$ Pa, and the plastic viscosity is $\mu = 75$ Pa ·s (with increasing yield stress τ_0, the nonlinearity of Eq. (4) gets more pronounced, which without any interventions, results in a larger numerical instability in the corresponding simulation). In Fig. 2a, the first part of Eq. (6) is plotted, namely $\dot{W}_{KE}(t)$, while in Fig. 2b, the second part of Eq. (6) is plotted, which is $\dot{W}_{\eta}(t)$ (in the small integrated illustration of Fig. 2a, $\dot{W}_{KE}(t)$ is also plotted relative to the SRF, c.f. Section 3.1). Although $\dot{W}_{\eta}(t)$ is always positive, the same does not apply to $\dot{W}_{KE}(t)$. That is, a negative $\dot{W}_{KE}(t)$ value can be obtained, which means a reduction in the kinetic energy.

Relative to the SRF (see Section 3.1), the concrete sample is stationary at time $t = 0$ s. As a consequence, the rate of work components $\dot{W}_{KE}(t)$ and $\dot{W}_{\eta}(t)$ begins at zero as shown in Fig. 2. With the start of rotation, some wave generation occurs due to the fact that the concrete sample is interacting with the helically shaped geometry of the mixing blades inside the drum. Depending on the Bingham parameters used τ_0, μ, drum charge volume V and drum rotational speed f, these wave phenomena will differ (height and distance between the helically shaped blades and overall drum geometry will most certainly also influence the waves). Usually in the end, these waves will subside, meaning $\dot{W}_{KE}(t)$ and $\dot{W}_{\eta}(t)$ will become more or less fixed, to the extent possible.

3.4. Time integration and average values

By time integrating Eq. (6) as shown with Eq. (7), only the latter part of the curves in Fig. 2 are utilized. The time integration starts at $t_1 = 10$ s as shown with the vertical lines in each illustration and ends at $t_2 = 20$ s.

$$P = \frac{1}{t_2 - t_1}\int_{t_1}^{t_2} \dot{W}(t)\, dt = P_{KE} + P_{\eta} \tag{7}$$

It should be clear that both terms P and $\dot{W}(t)$ represents rate of work (i.e. power) with the physical unit of watts. The former variable is a time averaged integration to get a well defined average value, while the latter variable represents an instantaneous value, valid at the time t.

To reiterate, the generation of P by Eq. (7) is most necessary to produce quantifiable values for analysis and comparison. Starting the integration at 10 s and not at 0 s is made due to the fact that equilibrium in power (as far as possible) is usually obtained after 10 s (see Fig. 2). It is interesting to note that for Eq. (7), then $P_{KE} \ll P_{\eta}$ and thus $P \approx P_{\eta}$. The exception for this applies to the high drum speed cases, in which the magnitude of P_{KE} can reach up to about 20% of P_{η}.

For the remainder of this work, power is calculated by the following equation:

$$P_t = P + P_0. \tag{8}$$

The term P is obtained by Eq. (7), while P_0 is a constant, here set equal to 2 kW. The value of P_0 is assumed to represent the power needed to rotate an empty drum. I.e., it represents the effect of the mechanical friction between the drum and the rest of the truck, e.g. from gearing box, bearing balls, carrying rollers and so forth. Its constant value of $P_0 = 2$ kW is arbitrarily chosen and could be higher or lower, depending on the concrete load as well as depending on the drum speed f as reported in Refs.[19,20].

4. Results and discussion

4.1. Power as a function of drum speed

Fig. 3 shows plots of the power P_t by Eq. (8) as a function of drum rotational speed f. These results apply to different rheological cases, namely yield stress τ_0 and plastic viscosity μ. In each illustration, labeled from (a) to (i), are three curves which apply to different drum charge volume V, nominally equal to 2.5 m^3, 5.4 m^3 and 8.2 m^3. Because of the addition P_0 in Eq. (8), the "y-axis" in Fig. 3 starts at 2 kW. It should be clear that the presence of P_0 will not affect the final conclusions of this work, it will however more or less eliminate the occurrence of negative G values, which will be explained shortly.

As to be expected, the outcome of Fig. 3 shows that the power P_t required to turn the drum increases with increased drum rotational speed f. However, the increase is not necessarily linear as shown in Fig. 3a, d and g. That is, for the combination of $V = 2.5$ m^3 and $\mu = 25$

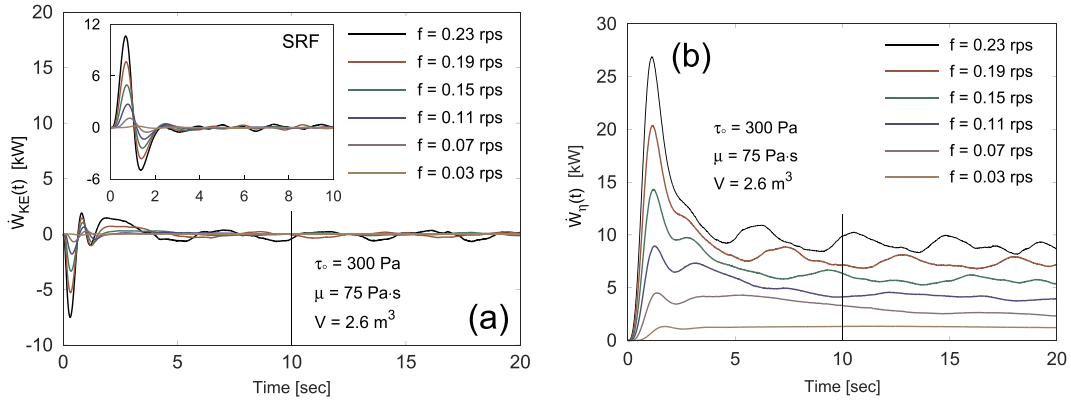

Fig. 2. Rate of work Eq. (6), $\dot{W}(t) = \dot{W}_{KE}(t) + \dot{W}_{\eta}(t)$, plotted as a function of time t.

Pa ·s, there is a small hump close to $f = 0.1$ rps, which disappears with increased volume V and plastic viscosity μ. This particular phenomenon was also present in Ref. [14] where it was further discussed.

In Fig. 3, it is interesting to note how the power results P_t for $V = 5.4$ m^3 are very close to the results of $V = 8.2$ m^3. This has to do with the balance between the quantity of concrete V that is being integrated in Eq. (6) and the magnitude of $\eta\,\dot{\gamma}^2$ in that same equation. For example, for the case of Fig. 3b at rotational speed $f = 0.19$ rps, the power values P_t of both volume cases do almost coincide. These two cases are shown in Fig. 4 at the instant of $t = 16.5$ s after start of rotation and show the cross-sections of $\eta\,\dot{\gamma}^2$. Although the domain of integration V is less for Fig. 4a ($V = 5.4$ m^3) the value of $\eta\,\dot{\gamma}^2$ is higher in that case, relative to the case of Fig. 4b ($V = 8.2$ m^3). That is, higher $\eta\,\dot{\gamma}^2$ values and smaller domain of integration V in Eq. (6), is often matched by lower $\eta\,\dot{\gamma}^2$ values and larger domain of integration V, resulting in similar power values P_t (from Eqs. (6) to (8)) for the two volume cases as observed in Fig. 3b.

Although the intensity of $\eta\,\dot{\gamma}^2$ is highest for the case of $V = 2.5$ m^3 (cross-section not shown), the domain of integration V in Eq. (6) is usually too small to reach the power values P_t of the case of $V = 5.4$ m^3 or $V = 8.2$ m^3.

In line with Refs. [17-20], the rheological parameters of the concrete mixing truck are represented with the slope H and the point of intersection with the ordinate G of the curves in Fig. 3, by linear regression. The corresponding model function is given by Eq. (9).

$$P_t = H\,f + G \tag{9}$$

In Fig. 5, the yield stress τ_0 and plastic viscosity μ (used in each simulation) are plotted as a function of the obtained G and H values (same types of illustrations are represented in Refs. [18-20]). In Fig. 5, the

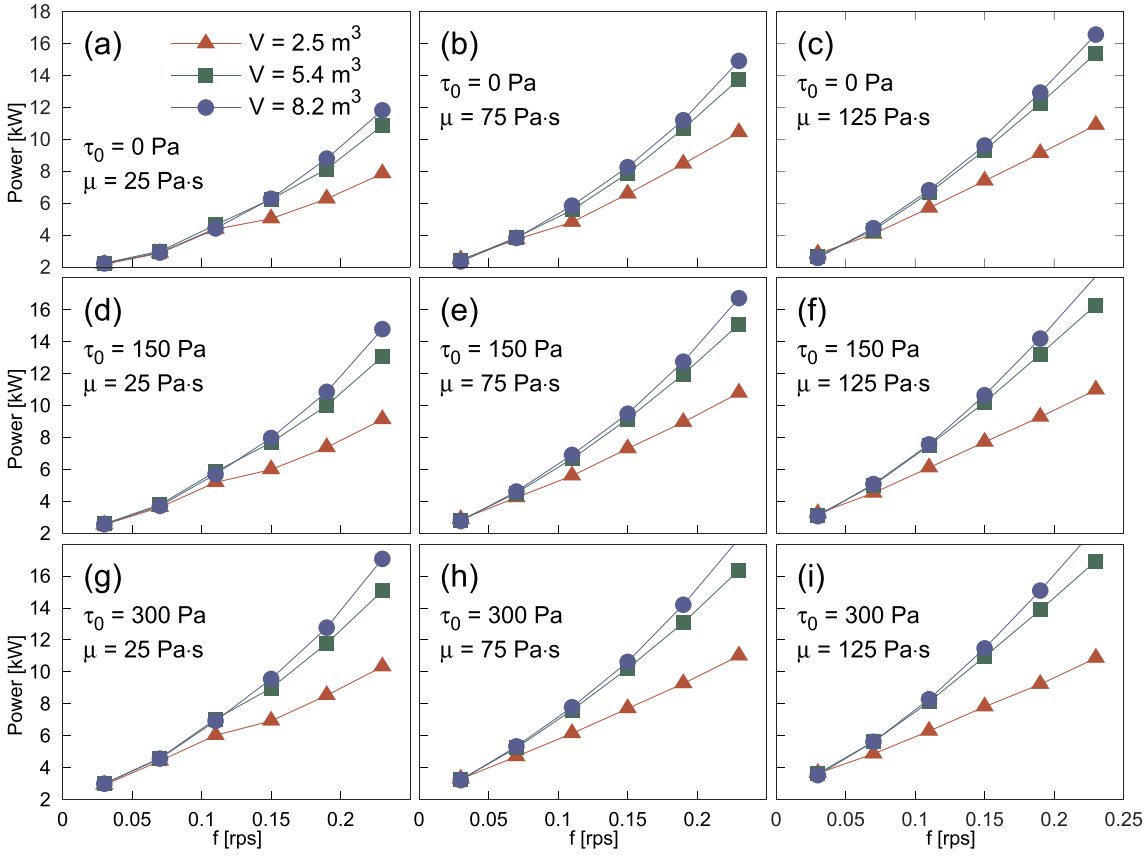

Fig. 3. Power P_t by Eq. (8) as a function of drum speed f for different conditions.

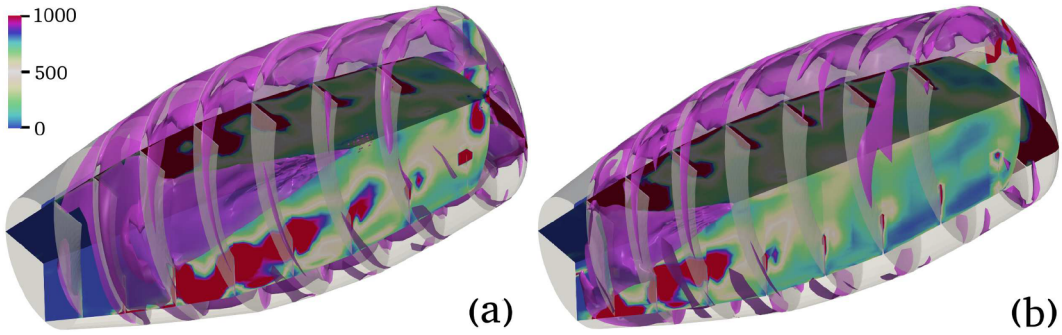

Fig. 4. Cross-section of $\eta\,\dot{\gamma}^2$ (in [Pa/s]) that applies for Fig. 3b at $f = 0.19$ rps and time $t = 16.5$ s, for the cases $V = 5.4$ m^3 (left) and $V = 8.2$ m^3 (right).

coefficient of determination for each volume case $V = 2.5$ m^3, 5.4 m^3 and 8.2 m^3 is represented with $R^2_{[2.5]}$, $R^2_{[5.4]}$ and $R^2_{[8.2]}$, respectively. As shown by these vales, adequate correlations can be obtained in some cases.

It should be noted that the G values in Fig. 5a are increased by a fixed value, namely 2 kW, due to the presence of P_0 in Eq. (8). The H values in Fig. 5b are however unaffected by P_0.

From Eqs. (8) and (9), then $P + P_0 = H\,f + G$, which means $P = H\,f + (G - P_0) = H\,f + G^*$. From the "$x$-axis" in Fig. 5a, it is clear that $G^* = G - P_0$ consist mostly of negative values. As already indicated, G^* represents the "G value" when there is no mechanical friction present between the drum and the rest of the truck (e.g. between the drum and the gearing box, ball bearings, carrying rollers and so forth). The G^* value is a result of linear regression of $P = P(f)$, with f ranging from 0.03 to 0.23 rps and is in general not equal to $P(0.03\text{ rps})$. This last mentioned value is here always positive, while G^* is in most cases not.

4.2. Specific power as a function of drum speed

To better understand the physical characteristics of the truck's rheological values shown in Fig. 5, the use of specific power (or power per unit mass) is appropriate, calculated by Eq. (10).

$$p_t = \frac{P_t}{m} = \frac{P_t}{\rho_1 V} \tag{10}$$

In the above equation, the term P_t comes from Eq. (8), while the term $m = \rho_1 V$ represents the mass [kg] of concrete inside the drum. Fig. 6 shows plots of the specific power p_t calculated by Eq. (10) as a function of drum rotational speed f.

As a proposal, the specific power is modeled with Eq. (11). By using the Nelder and Mead simplex algorithm [43], its parameters are $q_1 = 0.2420 \cdot 10^{-2}$ m^3/kg, $q_2 = 0.8226 \cdot 10^{-2}$ m^3/(kg ·s), $q_3 = -0.1916 \cdot 10^{0}$ 1/(m^4 ·s^2), $q_4 = -0.6847 \cdot 10^{1}$ m^3, $q_5 = 0.2227 \cdot 10^{2}$ m^5/s^2, $q_6 = 0.6892 \cdot 10^{-3}$ m^6/(kg ·s), $q_7 = 0.1959 \cdot 10^{1}$ m^8/s^3, $q_8 = -0.1195 \cdot 10^{2}$ kg ·m^4/s^4 and $q_9 = 0.7597 \cdot 10^{1}$ Pa·s, and found by simultaneous fitting all the data in Fig. 6.

$$p_t = \left(q_1\,\tau_0 + q_2\,\mu + q_3\,(V + q_4)^2 + \frac{q_5}{V}\right) f + \frac{q_6\,\tau_0 + q_7/V + q_8/(\mu + q_9)}{V} \tag{11}$$

As shown with Fig. 7, with the obtained parameters q_1 to q_9, Eq. (11) does not fully fit all the data points. Despite its limitations, this equation is sufficient to point out the main physical characteristics of the truck's rheological values, given below.

With Eqs. (9) and (10) in mind, then from Eq. (11), the G and H values of Fig. 3 can be directly obtained:

$$G = \rho_1 \left(q_6\,\tau_0 + \frac{q_7}{V} + \frac{q_8}{\mu + q_9}\right), \tag{12}$$

$$H = \rho_1 V \left(q_1\,\tau_0 + q_2\,\mu + q_3\,(V + q_4)^2 + \frac{q_5}{V}\right). \tag{13}$$

The first thing to note with the two above equations is that the truck's values G and H depend on the volume of concrete V in a non-linear fashion. Also, there is a linear dependency on the concrete density ρ_1, which originates from the use of Eq. (10).

As shown by Eq. (13), the slope H does not only depend on the plastic viscosity μ, but also on the yield stress τ_0. Although q_1 is lower than q_2 in Eq. (13), the yield stress τ_0 is often larger than the plastic viscosity μ. For example with $\tau_0 = 300$ Pa and $\mu = 25$ Pa ·s, then $q_1\,\tau_0 = 0.726$ m^2/s^2, which is larger than $q_2\,\mu = 0.206$ m^2/s^2. That is, the yield stress τ_0 can exert a larger influence on the slope H, relative to the plastic viscosity μ. This can explain the difficulty in correlating the H value only with μ, as reported in Refs. [18-20].

When considering Eq. (12), the plastic viscosity μ influences the G value through $q_8/(\mu + q_9)$. This term is nonlinear in such a manner that its effect will only diminish towards zero with increasing plastic viscosity μ. This is different from the effect of yield stress τ_0, which is ruled

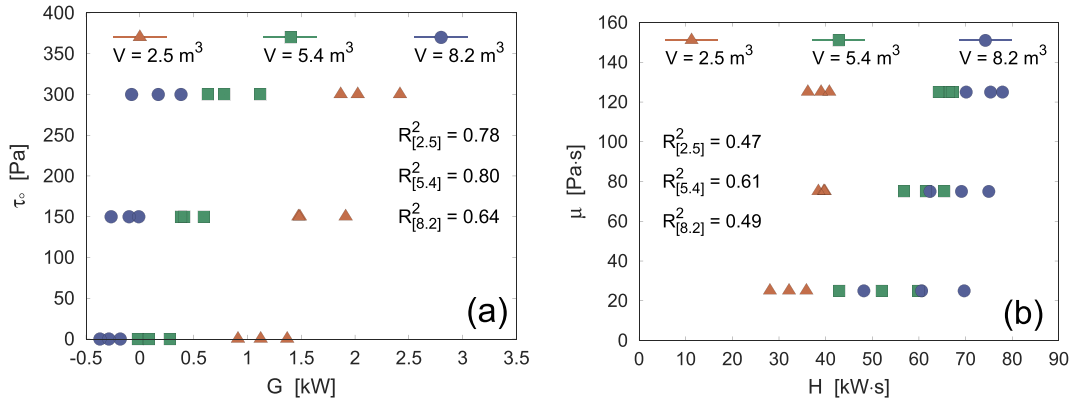

Fig. 5. Yield stress τ_0 and plastic viscosity μ versus G and H values for the cases in Fig. 3.

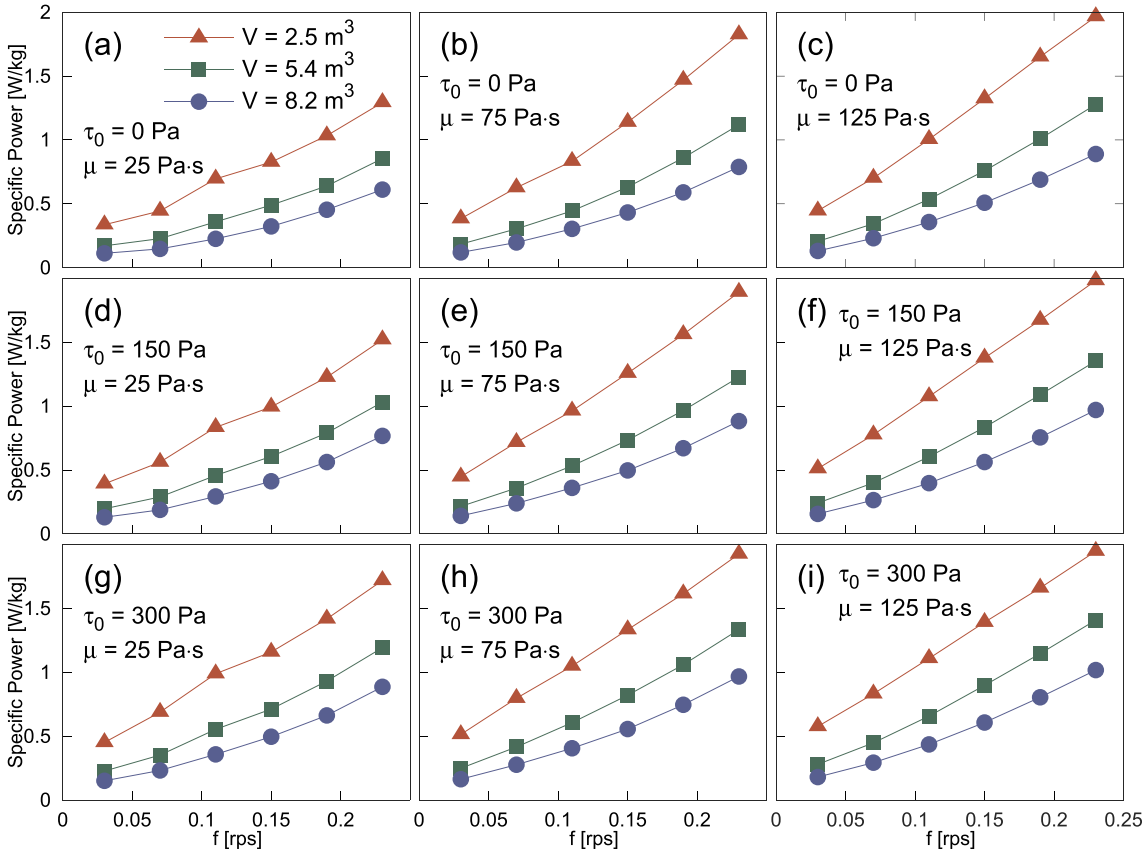

Fig. 6. Specific power p_t by Eq. (10) as a function of drum speed f.

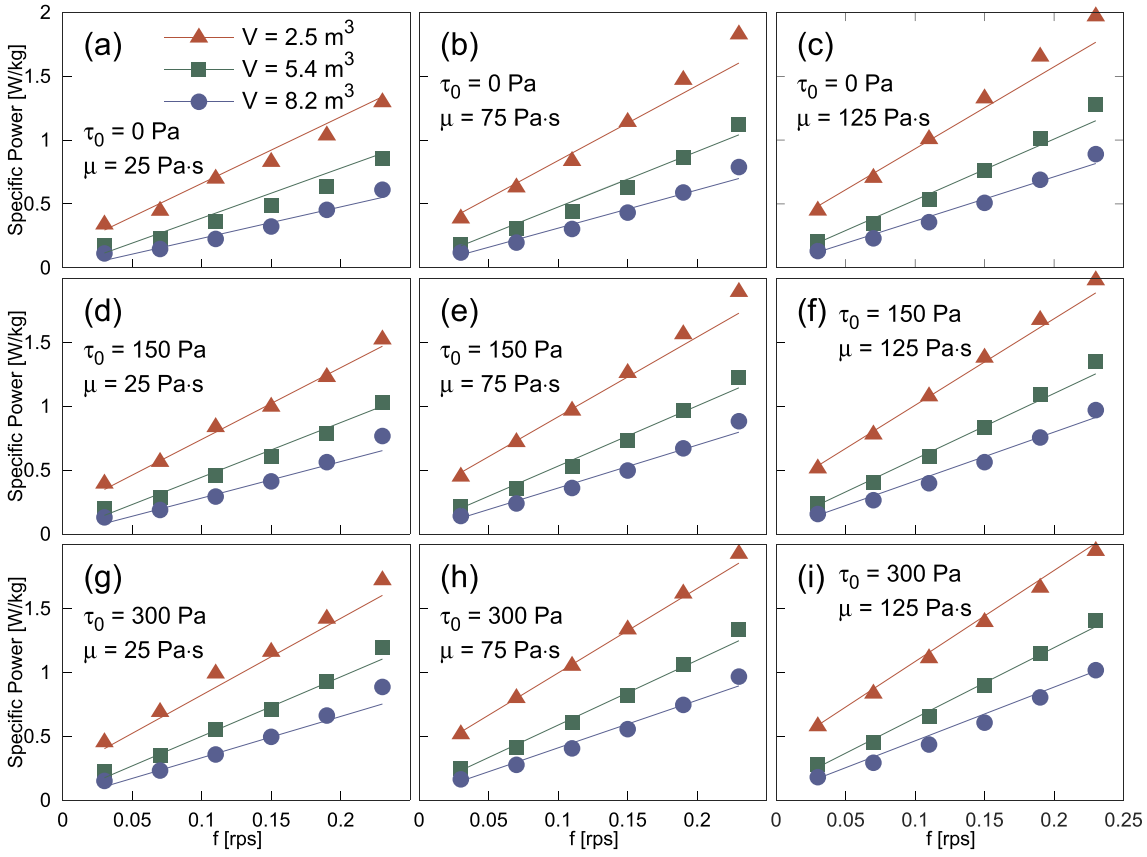

Fig. 7. Specific power p_t by Eq. (11) plotted against the data points in Fig. 6.

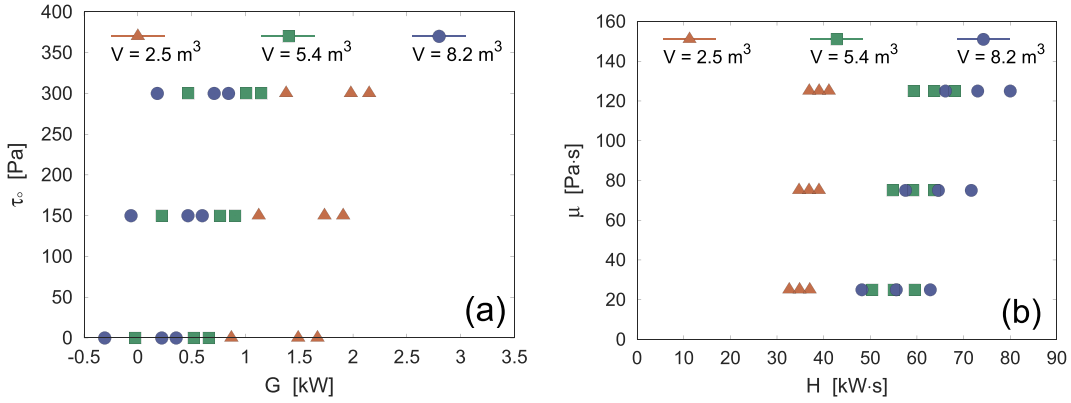

Fig. 8. Yield stress τ_0 and plastic viscosity μ versus calculated G and H values by Eqs. (12) and (13).

by the linear term $q_6\,\tau_0$. When increasing the yield stress τ_0, say from 25 to 125 Pa, it will result in 400% increase for $q_6\,\tau_0$, while increasing the plastic viscosity μ by the same value, from 25 to 125 Pa ·s, it will result in 75% reduction for the absolute value of $q_8/(\mu + q_9)$, which is a significantly smaller change. The above text can explain why it is possible to experimentally correlate the G value mostly to the yield stress τ_0, as for example reported in Refs. [18-20].

Fig. 8 shows the yield stress τ_0 and plastic viscosity μ versus G and H values calculated by Eqs. (12) and (13). By comparison, the correct τ_0-G and μ-H relationships are shown in Fig. 5. Clearly, Figs. 8 and 5 are somewhat dissimilar, demonstrating that Eqs. (12) and (13) are not complete.

5. Conclusions

In this work, the relationship between the power required to turn (i.e. spin) the drum of a concrete mixing truck and the rheological properties of the fresh concrete has been analyzed. Assuming a Bingham behavior, the power has been calculated for different cases of yield stress τ_0 and plastic viscosity μ. In line with Refs. [17-20], the resulting power curves (Fig. 3) were used in calculating the intersection value G and the slope H (see Eq. (9)), which then represents the truck's rheological values (Fig. 5). By using specific power instead of absolute power (see Eq. (10) and Fig. 6), it was possible to propose a relationship between the Bingham parameters τ_0 and μ and the truck's rheological values G and H, given by Eqs. (12) and (13). However, since the parent equation, namely Eq. (11), does not fully fit all the data points (Fig. 7), Eqs. (12) and (13) are not completely accurate. Nevertheless, the outcome can be used in explaining the physical characteristics of the truck's rheological values:

- Both the yield stress τ_0 and the plastic viscosity μ do influence the slope H, to similar or the same extent. This can explain why it has been difficult to experimentally correlate only the plastic viscosity μ to the H value, as reported in Refs. [18-20].
- Although the plastic viscosity μ affects the G value, its influence is only minor, which can explain why it has been easier (relatively to the above) to experimentally correlate yield stress τ_0 to the G value, as reported in Refs. [18-20].
- In addition to the above, the truck's rheological values G and H depend on the volume of concrete V in a nonlinear fashion, while the dependency on the concrete density ρ_1 is here only linear (c.f. Eqs. (12) and (13)).

Declaration of competing interest

The authors declare that they have no known competing financial interests or personal relationships that could have appeared to influence the work reported in this paper.

Acknowledgments

This work was supported by the Icelandic Research Fund – RANNIS (grant numbers 163382–051,163382–052,163382–053) andNorcem AS (Heidelberg Cement Group).

The simulations were performed on resources provided by the Icelandic High Performance Computing Centre at the University of Iceland.

References

[1] G.H. Tattersall, P.F.G. Banfill, The Rheology of Fresh Concrete, Pitman Books Limited, Great Britain, 1983 out of print but electronic copy available from P.F.G.Banfill@hw.ac.uk).
[2] N. Roussel, S. Staquet, L. D'Aloia Schwarzentruber, R. Le Roy, F. Toutlemonde, SCC Casting prediction for the realization of prototype VHPC-precambered composite beams, Mater. Struct. 40 (9) (2007) 877–887.
[3] L.N. Thrane, Form Filling with Self-Compacting Concrete, PhD thesis, Department of Civil Engineering Technical University of Denmark, 2007.
[4] J. Spangenberg, N. Roussel, J.H. Hattel, H. Stang, J. Skocek, M.R. Geiker, Flow induced particle migration in fresh concrete: theoretical frame, numerical simulations and experimental results on model fluids, Cem. Concr. Res. 42 (2012) 633–641.
[5] A. Gram, J. Silfwerbrand, B. Lagerblad, Obtaining rheological parameters from flow test. Analytical, computational and lab test approach, Cem. Concr. Res. 63 (2014) 29–34.
[6] K. Vasilic, W. Schmidt, H.C. Kuhne, F. Haamkens, V. Mechtcherine, N. Roussel, Flow of fresh concrete through reinforced elements: experimental validation of the porous analogy numerical method, Cem. Concr. Res. 88 (2016) 1–6.
[7] N. Roussel, A. Gram, M. Cremonesi, L. Ferrara, K. Krenzer, V. Mechtcherine, S. Shyshko, J. Skocec, J. Spangenberg, O. Svec, L.N. Thrane, K. Vasilic, Numerical simulations of concrete flow: a benchmark comparison, Cem. Concr. Res. 79 (2016) 265–271.
[8] O. Svec, J. Skocek, H. Stang, M.R. Geiker, N. Roussel, Free surface flow of a suspension of rigid particles in a non-Newtonian fluid: a lattice Boltzmann approach, J. Non-Newtonian Fluid Mech. 179-180 (2012) 32–42.
[9] V. Mechtcherine, A. Gram, K. Krenzer, J.H. Schwabe, S. Shyshko, N. Roussel, Simulation of fresh concrete flow using Discrete Element Method (DEM): theory and applications, Mater. Struct. 47 (2014) 615–630.
[10] N. Roussel, A. Gram (Eds.), Simulation of Fresh Concrete Flow, State-of-the Art Report of the RILEM Technical Committee 222-SCF Springer, 2014.
[11] J.E. Wallevik, Rheological properties of cement paste: thixotropic behavior and structural breakdown, Cem. Concr. Res. 39 (2009) 14–29.
[12] S. Tichko, J. Van De Maele, N. Vanmassenhove, G. De Schutter, J. Vierendeels, R. Verhoeven, P. Troch, Numerical simulation of formwork pressure while pumping self-compacting concrete bottom-up, Eng. Struct. 70 (2014) 218–233.
[13] K. Krenzer, J. Martin, U. Palzer, Development of a truck mixer simulator on a laboratory scale using CAD and simulation, CPI-Worldwide, Issue 1, 2014.
[14] J.E. Wallevik, O.H. Wallevik, Analysis of shear rate inside a concrete truck mixer, Cem. Concr. Res. 95 (2017) 9–17.
[15] K. Krenzer, V. Mechtcherine, U. Palzer, Simulating mixing processes of fresh concrete using the discrete element method (DEM) under consideration of water addition and changes in moisture distribution, Cem. Concr. Res. 115 (2019) 274–282.
[16] J.E. Wallevik, Relationship between the Bingham parameters and slump, Cem. Concr. Res. 36 (2006) 1214–1221.

[17] J.A. Daczko, A proposal for measuring rheology of production concrete, Concr. Int. 22 (5) (2000) 47–49.
[18] S. Amziane, C.F. Ferraris, E.P. Koehler, Measurement of workability of fresh concrete using a mixing truck, J. Res. Natl. Inst. Stand. Technol. 110 (2005) 55–66.
[19] S. Amziane, C.F. Ferraris, E.P. Koehler, Feasibility of using a concrete mixing truck as a rheometer, NISTIR (September 2006) 7333.
[20] C.F. Ferraris, R. Cooley, J. Grein, M. Peltz, M. Topputo, S. Verdino, Feasibility of using a concrete mixing truck as a rheometer (Orlando, Florida), NISTIR (September 2007) 7447.
[21] J.E. Wallevik, K. Krenzer, J.H. Schwabe, Numerical errors in CFD and DEM modeling, in: A. Gram, N. Roussel (Eds.), Simulation of Fresh Concrete Flow, Springer Netherlands, 2014.
[22] O.H. Wallevik, J.E. Wallevik, Rheology as a tool in concrete science: the use of rheographs and workability boxes, Cem. Concr. Res. 41 (12) (2011) 1279–1288.
[23] H.G. Weller, G. Tabor, H. Jasak, C. Fureby, A. tensorial approach to computational continuum mechanics using object-oriented techniques, Comput. Phys. 12 (1998) 620–631.
[24] C.W. Hirt, B.D. Nichols, Volume of fluid (VOF) method for the dynamics of free boundaries, J. Comput. Phys. 39 (1) (1981) 201–225.
[25] J. Klostermann, K. Schaake, R. Schwarze, Numerical simulation of a single rising bubble by VOF with surface compression, Int. J. Numer. Meth. Fluids 71 (8) (2013) 960–982.
[26] K. Kissling, J. Springer, H. Jasak, S. Schutz, K. Urban, M. Piesche, A coupled pressure based solution algorithm based on the volume-of-fluid approach for two or more immiscible fluids, in: J.C.F. Pereira, A. Sequeira (Eds.), Fifth European Conference on Computational Fluid Dynamics, ECCOMAS CFD 2010, June 2010, pp. 14–17 lisbon Portugal.
[27] D. Feys, J.E. Wallevik, A. Yahia, K.H. Khayat, O.H. Wallevik, Extension of the Reiner-Riwlin equation to determine modified Bingham parameters measured in coaxial cylinders rheometers, Mater. Struct. 46 (2013) 289–311.
[28] R.I. Tanner, K. Walters, Rheology: An Historical Perspective, Elsevier Science B.V., Netherlands, 1998.
[29] H.A. Barnes, J.F. Hutton, K. Walters, An Introduction to Rheology, Elsevier Science B.V., Netherlands, 1989.
[30] G.E. Mase, Schaums Outline Series: Theory and Problems of Continuum Mechanics, McGraw-Hill Inc., USA, 1970.
[31] L.E. Malvern, Introduction to the Mechanics of Continuous Medium, Prentice-Hall Inc., New Jersey, 1969.
[32] M. Bercovier, M. Engelman, A finite element method for incompressible non-Newtonian flows, J. Comput. Phys. 36 (1980) 313–326.
[33] A.J. Taylor, S.D.R. Wilson, Conduit flow of an incompressible, yield-stress fluid, J. Rheol. 41 (1) (1997) 93–101.
[34] G.R. Burgos, A.N. Alexandrou, V. Entov, On the determination of yield surfaces in Herschel-Bulkley fluids, J. Rheol. 43 (3) (1999) 463–483.
[35] J.E. Wallevik, Rheology of Particle Suspensions — Fresh Concrete, Mortar and Cement Paste with Various Types of Lignosulfonates, PhD thesis Department of Structural Engineering, The Norwegian University of Science and Technology, Trondheim, Norway, 2003https://ntnuopen.ntnu.no.
[36] J.E. Wallevik, Minimizing end-effects in the coaxial cylinders viscometer: visco-plastic flow inside the ConTec BML Viscometer 3, J. Non-Newtonian Fluid Mech. 155 (2008) 116–123.
[37] G.T. Mase, G.E. Mase, Continuum Mechanics for Engineers, second, CRC Press LLC, USA, 1999.
[38] E. Haug, H.P. Langtangen, Basic equations in Eulerian continuum mechanics, in: M. Dæhlen, A. Tveito (Eds.), Numerical Methods and Software Tools in Industrial Mathematics, Birkhauser, 1997.
[39] R.A. Brown, Fluid Mechanics of the Atmosphere, Academic Press, Inc., USA, 1991.
[40] J.E. Wallevik, Effect of the hydrodynamic pressure on shaft torque for a 4-blades vane rheometer, Int. J. Heat Fluid Flow 50 (2014) 95–102.
[41] Ansys Fluent 6.3 User's Guide 2006, ANSYS, Inc., USA, 2006.
[42] M.L. Salby, Fundamentals of Atmospheric Physics, Academic Press, 1996.
[43] J.A. Nelder, R. Mead, A simplex method for function minimization, Computer. J. 7 (1965) 308–313.